Research Square

Preprints are preliminary reports that have not undergone peer review.
They should not be considered conclusive, used to inform clinical practice,
or referenced by the media as validated information.

Light Perturbations Rapidly Reshape Community Structure and Functional Potential of Synechococcus and Its Co-occurring Bacterial Community in an Estuarine Ecosystem

Yuting Zhou
Yantai Institute of Coastal Zone Research
Ting Wang
Yantai Institute of Coastal Zone Research
Jialin Li
jlli@yic.ac.cn

Yantai Institute of Coastal Zone Research
Huiwang Gao
Ocean University of China
Song Qin
Yantai Institute of Coastal Zone Research

Research Article

Keywords: Synechococcus, Co-existing bacteria, Light responses, Dissolved organic carbon (DOC), Yellow River Estuary

Posted Date: October 27th, 2026

DOI: https://doi.org/10.21203/rs.3.rs-11340030/v1

License: This work is licensed under a Creative Commons Attribution 4.0 International License.
Read Full License

Additional Declarations: No competing interests reported.

Abstract

Estuarine ecosystems frequently experience rapid fluctuations in light availability, yet the short-term responses of microbial communities to such perturbations remain incompletely understood, particularly with respect to shifts in functional potential and organic matter cycling. Multi-omics and geochemical analyses were applied to examine microbial community responses during 24-h light/dark shipboard incubations using seawater from the Yellow River Estuary (YRE). The dominant *Synechococcus* OTU (OTU61), affiliated with S5.1 Clade IX, increased in relative abundance in both Light and Dark treatments relative to the *in situ* samples. Surface communities showed greater compositional turnover during incubation than bottom communities, as reflected by higher OTU loss rates (57.72% vs. 46.51%), though enclosure effects cannot be excluded as a contributing factor. Functional annotation of metagenomic data revealed differences in the relative representation of enzymes associated with carbon metabolism and redox processes between Light and Dark treatments. Metabolomic profiles and dissolved organic carbon (DOC) concentrations also varied between treatments, potentially reflecting differences in organic matter pools associated with light conditions. These results indicate concurrent changes in microbial community composition, functional gene representation, and metabolite profiles during short-term light perturbation in shipboard incubation. These observations provide an exploratory framework for understanding light-associated microbial processes in estuarine systems and highlight the need for further validation using direct process-based approaches.

Introduction

Marine phytoplankton are exposed to highly dynamic light environments shaped by tidal mixing [1], vertical water column structure [2], and variable weather patterns [3]. The selective absorption of photons by water molecules further constrains the spectral and intensity range available for photosynthesis [4], with light fluctuation in aquatic systems occurring over timescales of seconds to minutes at intensities an order of magnitude greater than those in terrestrial environments [5]. Among marine primary producers, picoplanktonic cyanobacteria, particularly *Synechococcus* and Prochlorococcus, are ubiquitous and ecologically significant, collectively accounting for approximately 25% of ocean net primary production (~ 12 Gt C yr^{-1}) [6]. *Synechococcus* alone contributes approximately 27% of total picophytoplankton carbon biomass globally and supports an estimated net primary production of 8 Gt C yr^{-1} [6, 7]. Beyond primary productivity, *Synechococcus* plays a key role in mediating carbon, nitrogen, and phosphorus cycling and contributes to dissolved organic matter (DOM) production and the biological carbon pump [8]. Light is a central driver of *Synechococcus* physiology and ecology: diel transcriptomic profiling revealed synchronized oscillations in genes related to photosystem activity, energy metabolism, and carbon fixation [9], highlighting the sensitivity of this organism to short-term light variability. These light-driven shifts in *Synechococcus* physiology and metabolism are unlikely to occur in isolation; rather, they may propagate to the surrounding microbial community through changes in the quantity and composition of released DOM.

Phytoplankton light responses often cascade to their surrounding microenvironment (the phycosphere), altering the quantity and quality of released DOM and other microchemical conditions that directly shape associated bacterial assemblages [10, 11]. Such associations between phytoplankton and bacteria are fundamental to marine food web dynamics and global biogeochemical cycling [12, 13]. *Synechococcus* is rarely found in isolation in natural environments; even under laboratory culture conditions, it is typically accompanied by co-occurring heterotrophic bacteria [14–16]. These associations involve reciprocal influences on physiology and metabolism: *Synechococcus* releases compositionally distinct DOM that may shape associated microbial communities [17, 18], while heterotrophic bacteria in turn affect *Synechococcus* growth and nutrient availability [19, 20]. Beyond indirect effects mediated through DOM, heterotrophic bacteria can also respond directly to light through light-utilizing systems such as proteorhodopsins and bacteriochlorophyll a, based phototrophy in aerobic anoxygenic phototrophs (AAP), which may modify bacterial growth and metabolic potential under different light regimes [21–23]. Accordingly, these observations suggest that light availability may simultaneously drive shifts in *Synechococcus* physiology and the composition of its co-occurring bacterial community. Such light-mediated interactions are particularly relevant in dynamic estuarine environments, where light availability fluctuates rapidly due to tidal mixing and episodic sediment loading, yet how these responses unfold over short timescales in such settings remains poorly understood.

The Yellow River Estuary (YRE) represents one of the most dynamic and ecologically significant transitional zones between terrestrial and marine environments in China, receiving substantial freshwater, sediment, and nutrient inputs from China's second-longest and sixth-longest river in the world [24, 25]. The Water-Sediment Regulation Scheme (WSRS), implemented to manage sediment accumulation in the lower Yellow River, delivers massive sediment loads within short periods, dramatically reducing underwater light availability and reshaping phytoplankton community structure [26, 27]. Simultaneously, the WSRS substantially elevates near-shore concentrations of dissolved inorganic nitrogen (DIN), dissolved inorganic phosphorus (DIP), and chemical oxygen demand (COD), pushing the system toward moderate-to-severe eutrophication [24] and creating a new condition of "eutrophication under P-limitation" that favors longer-lasting and more frequent harmful algal blooms [27]. Moreover, the abrupt changes in hydrology, optical properties, and nutrient stoichiometry imposed by the WSRS exert strong controls on phytoplankton community structure and species succession [26]. Under these conditions of elevated nutrient loading, altered light climate, and hydrological disturbance, *Synechococcus* has emerged as an ecologically important picocyanobacterium in estuarine systems, with accumulating evidence suggesting bloom potential under eutrophic, low-phosphorus, or high dissolved organic matter conditions [28, 29]. In the YRE, where light availability fluctuates abruptly in response to WSRS-driven sediment pulses, understanding how *Synechococcus* and its co-occurring heterotrophic bacterial community respond to short-term irradiance changes is therefore of both ecological and biogeochemical relevance. Despite this relevance, community-level microbial responses to such short-term light perturbations in the YRE remain poorly characterized, particularly with respect to simultaneous shifts in community composition, functional gene representation, and metabolite profiles.

Previous studies have shown that *Synechococcus* exhibits pronounced physiological and ecological responses to light/dark cycles, including diel rhythms in growth, cell division, and gene representation, as well as shifts in community composition under altered light regimes [30, 31]. However, most of this knowledge derives from controlled laboratory experiments using simplified assemblages or model strains under stable light conditions. How natural *Synechococcus* populations and their co-occurring heterotrophic bacterial communities respond to abrupt, short-term light perturbations, as occur during WSRS-driven sediment pulses in the YRE, remains poorly characterized at the community and functional gene level. In particular, simultaneous multi-omics characterization of community composition, functional gene representation, and metabolite profiles during such perturbations has rarely been attempted in estuarine settings. Against this background, this study conducted 24-hour shipboard light/dark incubation experiments using surface and bottom seawater collected from 3 stations in the YRE, integrating metagenomic, metabolomic, and geochemical analyses. Given the exploratory nature of the study design, in which samples from the 3 stations were pooled to obtain sufficient biomass for omics analyses, the following working hypotheses are proposed to guide interpretation rather than formal hypothesis testing. Light and dark conditions are expected to be associated with distinct functional profiles of *Synechococcus* and co-occurring bacterial communities, as well as differences in the overall microbial metabolite profiles. Differences in initial community composition and environmental conditions between surface and bottom waters are expected to result in distinct response patterns between depths. Metabolite profiles and dissolved organic carbon concentrations are anticipated to differ between light and dark treatments, reflecting light-associated differences in organic matter dynamics. This study aims to provide an exploratory, community-level characterization of microbial responses to short-term light perturbation in a hydrologically dynamic estuarine system, generating hypotheses for future process-based investigations.

Materials and methods

Field sampling

The seawater employed in all incubation experiments was meticulously procured from stations A3 (38°17’N, 119°13’E), B2 (37°59’N, 119°15’E), and E2 (37°38’N, 119°28’E) within the Bohai Sea during the R/V Chuangxin Yi expedition, spanning the dates from July 18 to 22, 2022, coinciding with the post-WSRS recovery period (Fig. 1). This seawater was meticulously collected from both surface and bottom layers, utilizing the state-of-the-art shipborne CTD system manufactured by Seabird, USA. The water depths at stations A3, B2, and E2 were 22.5 m, 15 m, and 13.7 m, respectively. Surface and bottom water temperature, salinity, and turbidity at sampling stations affected by the Yellow River discharge are summarized in Table 1.

Table 1
Surface and bottom temperature, turbidity, and salinity data measured at the 3 stations.

Water column	Stations	Temperature/℃	Turbidity/NTU	Salinity/PSU
Surface water	A3	21.31	0.76	26.58
	B2	21.68	6.98	24.63
	E2	27.69	11.21	35.61
Bottom water	A3	19.86	8.39	30.32
	B2	23.12	7.69	29.51
	E2	26.52	11.45	26.53

Incubation experiments and sample collection

1000 milliliters of seawater, sampled from both the surface and bottom layers at A3, B2, and E2 stations, were subjected to a rigorous filtration process employing a nylon mesh with a pore size of 48 μm. The filtered seawater was subsequently transferred into 2000 mL polycarbonate culture bottles (Thermo Scientific Nalgene™, 2105 – 2000) and incubated for 24 hours under natural light and dark conditions. For the dark treatment, each bottle was completely wrapped with aluminum foil (Aluminum Foil MF50; MiaoJie Co., China), which provides 100% light exclusion. To minimize eukaryotic grazing effects, filter-sterilized cycloheximide (CHX) was added to each culture bottle at a final concentration of 50 $mg{\cdot}L^{-1}$ [32]. After the incubation experiments, seawater was collected and filtered through 0.22 μm-pore-size polycarbonate filters (Millipore Co., Bedford, MA, USA). The filtrate and filters were kept at -80℃ until further analyses of the metabolite and planktonic communities included both *in situ* and cultured samples. To capture a generalized community-level response to light conditions across the YRE sampling sites, filters from the same treatment across the three stations were cut into small pieces and pooled prior to DNA extraction; the corresponding filtrates were similarly pooled for metabolomic analyses. This pooling approach was adopted to obtain sufficient biomass and dissolved organic matter for downstream omics analyses and to derive a spatially integrated signal across stations. Consequently, each treatment condition was represented by a single pooled composite sample for metagenomic, and metabolomic analyses, with no independent biological replicates available for these datasets. All omics-based comparisons between treatments should therefore be interpreted as exploratory and hypothesis-generating rather than statistically confirmatory. Nutrient and dissolved organic carbon (DOC) concentrations were measured independently for each station and treatment, providing replicated geochemical observations that support quantitative comparisons between light and dark conditions. Surface and bottom seawater collected directly from each station prior to incubation served as *in situ* reference samples, denoted as S and B, respectively. Incubation treatments were established for both depths: surface seawater incubated under natural light was labeled SL, and surface seawater incubated in darkness was labeled SD. Similarly, bottom seawater incubated under natural light

was designated BL, and bottom seawater incubated in darkness was designated BD. For subsequent analyses, S and B are referred to as the *in situ* reference (ISR) group, SL and BL as the Light group, and SD and BD as the Dark group.

Nutrient concentrations in all samples, including both *in situ* samples and culture treatments, were determined after filtering 50 mL of seawater through 0.45 μm syringe filters (JINTENG Co., China). The filtrates were collected in transparent plastic bottles for the analysis of nitrates (NO_3^-), nitrites (NO_2^-), ammonium (NH_4^+), phosphates (PO_4^{3-}), and silicate (SiO_3^{2-}). For dissolved organic carbon (DOC) collection, seawater samples from both *in situ* and culture treatments were filtered through 0.45 μm syringe filters (JINTENG Co., China). The filtrates were stored in brown glass bottles that had been pretreated by soaking in 40% hydrochloric acid and combusted at high temperature in a muffle furnace before use.

Determination of inorganic nutrients and DOC

Concentrations of dissolved inorganic nutrients were quantified using flow injection analysis (QuAAtro, Bran+Luebbe, Germany) after thawing the samples at 4℃. The determination of DOC was carried out concerning the method in Chinese national standard GB17378.4-2007. The specific operation is as follows. The sample was automatically fed into the total carbon (TC) combustion tube (equipped with platina catalyst, 680℃) through the injector, and the carbon-containing organic matter in the sample was oxidized to carbon dioxide by passing high-purity air and then quantified by a non-dispersive infrared detector. Then the same water sample was automatically injected into the inorganic carbon (IC) reactor (equipped with 25% phosphoric acid solution), and the carbon dioxide generated by acidifying the inorganic carbonate at room temperature was detected by a non-dispersive infrared detector to determine the inorganic carbon content, and the total organic carbon (TOC) content is obtained by subtracting the inorganic carbon from the total carbon.

Measurement of metabolites

LC-MS-based untargeted metabolomics was used to identify metabolite differences between *in situ* seawater samples and those cultured for 24 hours under different light conditions. A 1 mL sample was collected and put into freeze-drying machine, and then 100 μL 80% methanol aqueous solution was added to freeze-dried powder. The obtained solution was subjected to vortex oscillation, fully mixed, and then placed in an ice bath for 5 min, followed by centrifugation at 15,000×g, 4 ℃ for 15 min. A certain amount of supernatant was moved, and mass spectrometry grade water was added to dilute the methanol content in the supernatant to 53%. The diluted supernatant was then centrifuged again at 15,000 × g for 15 min at 4°C, and the final supernatant was subjected to LC-MS analysis using a Vanquish ultra-high-performance liquid chromatography (UHPLC) system coupled with an Orbitrap Q Exactive™ HF mass spectrometer (Thermo Fisher, Germany).

DNA extraction and metagenomic sequencing

For DNA extraction, the membranes were cut into pieces, and then the DNA was extracted using the Invitrogen DNA Extraction Mini kit (Invitrogen, Thermo Fisher Scientific, Carlsbad, CA, USA), following the manufacturer's instructions. The genomic DNA was randomly sheared into short fragments. The obtained fragments were end-repaired, a-tailed, and further ligated with an Illumina adapter. The fragments with adapters were PCR amplified, size selected, and purified. The library was checked with Qubit 2.0 (Life Technologies, CA, USA), real-time PCR for quantification, and a bioanalyzer for size distribution detection. Quantified libraries will be pooled and sequenced on Illumina platforms, according to effective library concentration and data amount required. The extracted DNA was sequenced by Novogene Co., Ltd. (Beijing, China) using the HiSeq sequencing platform.

Metagenomic data process

Raw metagenomic data obtained from the Illumina HiSeq sequencing platform were preprocessed using Readfq V8.0 to generate clean Data for subsequent analysis. Clean data were assembled using MEGAHIT v1.0.4-beta, and the resulting Scaffolds were split at N junctions to obtain N-free Scaftigs. Open reading frames (ORFs) were predicted from the scaftigs using MetaGeneMark. Predicted genes from all samples were combined and clustered to remove redundancy, thereby constructing a non-redundant gene catalogue. Representative sequences from each cluster were defined as unigenes. DIAMOND was used to compare unigenes with the KEGG database for comparative analysis of metabolic pathways [33].

To characterize bacterial community composition, 16S rRNA gene sequences were extracted from the shotgun metagenomic reads using Metaxa2 [34] and clustered against the SILVA database (v132, 99% reference OTUs) using VSEARCH at a 97% sequence similarity threshold to generate an OTU table with QIIME 1.9.1 [35]. The 16S rRNA sequence of *Synechococcus* was removed, and the remaining bacterial sequences were compared with the FAPROTAX database to obtain the functional prediction results of the bacterial community. It should be noted that FAPROTAX predictions are based on taxonomic identity rather than direct functional measurements, and therefore reflect inferred functional potential rather than confirmed metabolic activity.

Results

Variations in inorganic nutrients and DOC concentration

As illustrated in Fig. 2, the three stations exhibited distinct vertical stratification in nutrient and DOC profiles under *in situ* conditions. At station A3, phosphate concentration was higher in surface waters (0.16 μmol•L^{-1}) compared to the bottom layer (0.09 μmol•L^{-1}), whereas ammonium (1.29 vs. 0.64 μmol•L^{-1}), nitrite (0.07 vs. 0.04 μmol•L^{-1}), silicate (6.28 vs. 4.66 μmol•L^{-1}), nitrate (0.29 vs. 0.08 μmol•L^{-1}), and DOC (3.22 vs. 2.07 mg•L^{-1}) concentrations were elevated in bottom waters. In contrast,

station B2 showed higher concentrations of phosphate (0.05 vs. 0.01 μmol•L⁻¹), ammonium (2.18 vs. 1.93 μmol•L⁻¹), nitrite (0.14 vs. 0.09 μmol•L⁻¹), silicate (10.66 vs. 4.42 μmol•L⁻¹), and nitrate (3.81 vs. 0.94 μmol•L⁻¹) in surface waters, while DOC remained slightly higher at the bottom (3.23 vs. 2.70 mg•L⁻¹). At station E2, all measured parameters exhibited higher concentrations in bottom waters, including phosphate (0.07 vs. 0.06 μmol•L⁻¹), ammonium (2.97 vs. 2.65 μmol•L⁻¹), nitrite (0.18 vs. 0.16 μmol•L⁻¹), silicate (17.93 vs. 14.70 μmol•L⁻¹), nitrate (4.87 vs. 4.31 μmol•L⁻¹), and DOC (5.77 vs. 2.05 mg•L⁻¹). Consistently, DOC concentrations at all three stations were elevated in the bottom layer, with average values approximately 1.8 times higher than those observed in the top layer.

Following a 24-hour incubation period, changes in nutrient concentrations and DOC were observed in both the surface and bottom layers. To assess these changes, the mean concentrations of nutrients and DOC were calculated under different light conditions for each layer at all 3 stations, and compared against *in situ* values. In surface seawater cultures (SL and SD), the concentrations of all nutrients, except for NH_4^+, were higher than those of the *in situ* samples (S). Conversely, in the bottom seawater cultures (BL and BD), only the DOC concentration increased relative to the *in situ* samples (B), while all nutrient concentrations, except for NH_4^+, decreased. Among the measured parameters, DOC exhibited the largest magnitude of change after 24 h. Relative to the corresponding *in situ* values, DOC concentrations in SL, SD, BL, and BD increased by 15.08-, 17.69-, 6.86-, and 8.55-fold, respectively, corresponding to net increases of 32.02, 37.96, 23.86, and 30.73 mg•L⁻¹, respectively. Comparison between natural light and dark conditions showed minimal differences in NO_2^- concentrations, whereas slight variations were noted in the other nutrients. DOC concentrations were numerically higher under dark conditions than under natural light in both surface and bottom waters; however, these differences were not statistically significant.

LC-MS metabolic profiles

Data analysis of the metabolic profiles across the three treatment groups revealed 246 metabolites. The Principal component analysis (PCA) scores of the metabolic profiles for different treatments (Fig. 3a) indicated that the PC1 axis accounted for 82.06% of the total data variance. The metabolic profile of the *in situ* seawater was distinctly separated from that of the samples cultured for 24 hours. The PC2 axis accounted for 6.82% of the total data variance. The PC2 axis distinguished the metabolic profiles of surface and bottom *in situ* samples, as well as those of the Light group from the Dark group.

To characterize the metabolic difference among the 3 groups, metabolites with |log2FC| >1 were selected as differentially abundant metabolites. The metabolic profiles of the Light and Dark groups were compared with that of the ISR group, which consisted of *in situ* seawater. Table S1 lists the differentially abundant metabolites between the Light group and the ISR group, with 55 metabolites up-regulated and 128 were down-regulated (Fig. 3b). Table S2 presents the differentially abundant metabolites between the Dark group and the ISR group, with 46 metabolites up-regulated and 137 down-regulated (Fig. 3c). In both comparisons, the up-regulated metabolites were mainly Benzenoids, Organic

acid and derivatives, and Organoheterocyclic compounds, whereas the down-regulated metabolites were mainly Lipids and lipid-like molecules, Organic acid and derivatives, Organoheterocyclic compounds, and Benzenoids. Specifically, in Light vs. ISR, the up-regulated metabolites comprised Benzenoids (9), Organic acid and derivatives (7), and Organoheterocyclic compounds (7), and the down-regulated metabolites comparised Lipid and lipid-like molecules (21), Organic acid and derivatives (20), Organoheterocyclic compounds (16), and Benzenoids (14); in Dark vs. ISR, the up-regulated metabolites comprised Benzenoids (7), Organoheterocyclic compounds (7), and Organic acids and derivatives (6), and the down-regulated metabolites comprised Lipid and lipid-like molecules (25), Organic acids and dervatives (23), Benzenoids (17), and Organoheterocyclic compounds (17). Table S3 lists the differentially abundant metabolites between the Light and Dark groups, with 8 metabolites up-regulated and 1 down-regulated. The 8 up-regulated metabolites were Cyclohexaneacetic acid, trans-2-Butene-1,4-dicarboxylic Acid, Capric acid, 4-Butylresorcinol, 12,13-EODE, Naringin, Isoproterenol, and 10-Hydroxydecanoic acid, while the down-regulated metabolite was Riboflavin (Fig. 3d).

Metagenomic overview

A total of six metagenomic libraries were constructed. Sequencing statistics for all samples are summarized in Table S4. Raw sequencing data ranged from 11,981.06 to 12,875.42 Mbp across all samples. After quality filtering, clean data ranged from 11,970.67 to 12,869.66 Mbp, with effective rates exceeding 99.9% in all samples, indicating minimal data loss during quality control. The Q20 and Q30 values of clean reads were consistently high, ranging from 96.37% to 97.12% and from 90.53% to 92.24%, respectively, demonstrating robust sequencing quality. GC content ranged from 41.57% to 52.75%, with surface-layer samples (S, SL, SD) consistently showing higher GC content than bottom-layer samples (B, BL, BD), suggesting that the inherent differences in microbial community composition between the two water layers were maintained even after 24 hours of light or dark incubation. De novo assembly of the quality-filtered reads yielded scaftigs ranging from 407.45 to 521.54 Mbp in total length, with N50 values between 1,187 and 1,378 bp across all samples (Table S5). Average contig lengths were broadly consistent across all treatments (1,107.90–1,206.53 bp), suggesting comparable assembly quality among groups. A non-redundant gene catalogue was subsequently constructed from all assembled sequences, comprising 2,000,057 predicted open reading frames (ORFs) with a total length of 1,217.03 Mbp and an average gene length of 608.5 bp. Among these, 36.31% were complete ORFs, while 22.55%, 28.46%, and 12.68% were end-incomplete, start-incomplete, and both-end-incomplete, respectively. The overall GC content of the gene catalogue was 46.95%. Rarefaction analysis based on the pan-gene curve showed that the cumulative number of non-redundant genes reached a plateau as the number of samples increased, indicating that the current sampling and sequencing depth were sufficient to capture the gene diversity of the microbial community and that additional samples would contribute few novel genes (Fig. S1).

The 2,000,057 ORFs in the non-redundant gene catalogue were functionally annotated against multiple databases, including KEGG, eggNOG, and CAZy. KEGG annotation assigned genes to six major functional categories (Fig. S2). Within the Metabolism category, the largest number of genes were associated with

amino acid metabolism (72,326 genes), followed by carbohydrate metabolism (68,653 genes), metabolism of cofactors and vitamins (47,833 genes), energy metabolism (46,222 genes), and nucleotide metabolism (39,118 genes). Within Environmental Information Processing, membrane transport (27,773 genes) and signal transduction (22,570 genes) were the most represented subcategories. Within Genetic Information Processing, translation-related genes were the most abundant (30,173 genes), followed by replication and repair (22,327 genes) and folding, sorting and degradation (17,679 genes). eggNOG annotation further characterized the functional profile of the gene catalogue across 24 COG categories (Fig. S3). The largest proportion of genes fell into the “Function unknown” category (S, 262,382 genes), which is common in metagenomic studies of marine environments. Among functionally characterized categories, amino acid transport and metabolism (E, 85,828 genes) was the most abundant, followed by cell wall/membrane/envelope biogenesis (M, 64,937 genes), energy production and conversion (C, 61,140 genes), replication, recombination and repair (L, 60,864 genes), and translation, ribosomal structure and biogenesis (J, 54,310 genes), consistent with the KEGG annotation results. CAZy annotation revealed that the gene catalogue contained 41,035 carbohydrate-active enzyme (CAZyme) genes distributed across six classes (Fig. S4). Glycosyl transferases (GT) represented the most abundant class with 17,186 genes, followed by glycoside hydrolases (GH, 14,226 genes) and carbohydrate-binding modules (CBM, 6,140 genes). Carbohydrate esterases (CE, 2,377 genes), auxiliary activities (AA, 745 genes), and polysaccharide lyases (PL, 361 genes) were comparatively less represented, suggesting that polysaccharide synthesis and degradation are both active processes within the sampled microbial communities.

Variety in lineages and relative abundance of Synechococcus

The relative abundance of *Synechococcus* was 2.22% in the ISR group, 4.34% in the Light group, and 4.44% in the Dark group. Compared to the ISR group, the relative abundance of *Synechococcus* increased in the Light and Dark groups, with an increase of 95.52% and 99.86%, respectively. Interestingly, when light conditions were altered from the *in situ* state, the relative abundance of *Synechococcus* showed larger changes in the treatments where illumination conditions were reversed. Specifically, switching surface samples to darkness (SD vs ISR-S) resulted in a 217.57% increase in *Synechococcus* relative abundance, compared to only a 28.44% increase under maintained light (SL vs. ISR-S). Similarly, exposing bottom samples to light (BL vs ISR-B) corresponded to a 174.92% increase, whereas incubation under continued darkness (BD vs. ISR-B) corresponded to a 39.48% decrease.

A total of 90 *Synechococcus* OTUs were detected across all samples. To avoid overlooking OTUs that were locally abundant in individual samples but ranked low in overall abundance, the top 10 *Synechococcus* OTUs by relative abundance were selected independently from each of the 6 samples. After removing duplicates, this yielded 14 unique OTU sequences for phylogenetic analysis. These sequences were aligned with the 16S rRNA sequences of known *Synechococcus* strains to construct a phylogenetic tree, which revealed affiliated with *Synechococcus* subcluster 5.1 clades I, II, III, V, VI, VII, VIII, IX, WPC1, and WPC2 (Fig. 4). Among these, OTU61 was the dominant OTU, affiliated with S5.1 clade IX, followed by OTU415 and OTU483, affiliated with S5.1 clade I and S5.1 clade II, respectively. Compared

to the ISR group, the relative abundance of OTU61, OTU415, and OTU483 showed increases in both the Light and Dark groups. In the Light group, the relative abundance of the 3 OTUs increased by 90.64%, 90.21%, and 107.01%, respectively, while in the Dark group, the corresponding increases were 106.34%, 93.12%, and 67.28%, respectively.

Diversity of co-occurring bacterial communities

The diversity and community structure of co-occurring bacterial communities are shown in Fig. 5. Shannon index values ranged from 6.16 (SD) to 6.55 (SL) across all samples, with differences observed among incubation treatments (Fig. 5a). The OTU level of the Venn analysis revealed that the surface (S) and bottom (B) of the *in situ* sample shared 1112 OTUs, whereas the number of OTUs exclusive to the surface and bottom layers was 1077 and 993, respectively. After 24 hours of incubation, the surface and bottom samples lost 57.72% and 46.51% of OTU, respectively. In surface seawater (SL and SD), the percentage of common OTUs was 44.15%, whereas the percentage of unique OTUs was 55.65%, based on a comparison of natural light and dark circumstances. In the bottom seawater (BL and BD), the percentage of common OTUs was 51.42%, while the percentage of unique OTUs was 48.57% (Fig. 5b). The Principal Coordinates Analysis (PCoA) showed that the first 2 axes explained 90.15% of the variance in bacterial community composition among samples (Fig. 5c). Axis 1 separated the *in situ* samples and the bottom seawater incubation samples from the surface incubation samples (69.47% interpretation); Axis 2 separated the surface light incubation sample from other samples (20.68% interpretation).

To elucidate the dynamics of bacterial community structure over the 24-hour incubation period, the proportions of various taxa relative to the total sequencing reads were calculated for both ISR and treatment groups (Fig. 5d and 5e). The bacterial composition of *in situ* seawater samples (S and B) was essentially similar; however, after 24 hours, various degrees of change occurred. Throughout the incubation period, Proteobacteria and Bacteroidetes emerged as predominant phyla in both ISR and treatment samples, exhibiting average relative abundances of 61.87% and 14.08%, respectively (Fig. 5d). When comparing the Light group to the ISR group (Light vs ISR), the relative abundances of Proteobacteria, Bacteroidetes, and Marinimicrobia decreased by 10.43%, 2.46%, and 78.86%, respectively, whereas Actinobacteria, Cyanobacteria, and Planctomycetes increased by 58.78%, 59.33%, and 196.89%. In contrast, in the Dark group relative to the ISR group (Dark vs ISR), Bacteroidetes and Actinobacteria exhibited trends opposite to those in the Light vs ISR, while the other four phyla showed similar patterns: Proteobacteria, Actinobacteria, and Marinimicrobia decreased by 3.21%, 1.56%, and 67.15%, respectively, whereas Bacteroidetes, Cyanobacteria, and Planctomycetes increased by 0.19%, 81.78%, and 39.48%. Direct comparison between the Light group and Dark group (Light vs Dark) revealed increases only in Actinobacteria (61.29%) and Planctomycetes (112.85%), while the relative abundances of all other phyla were lower in the natural light treatment. At the class level, the most abundant taxa were *α*-Proteobacteria, *γ*-Proteobacteria, and Bacteroidia, with average relative abundances of 33.31%, 26.76%, and 13.10%, respectively (Fig. 5e). After 24 h of incubation, the relative abundance of *α*-Proteobacteria decreased in both treatments, but to varying extents (-44.88% in light and − 6.89% in dark). In contrast, *γ*-Proteobacteria increased by 58.37% and 10.23% in the light and dark treatments,

respectively, and Bacteroidia also increased in both treatments (by 3.74% and 6.17%). Notably, *γ*-Proteobacteria increased by 43.67% in the direct comparison of Light vs Dark.

Functional potential of Synechococcus and bacteria communities

The inferred functional categories of *Synechococcus* co-occurring bacterial communities based on FAPROTAX annotation included carbon (C), nitrogen (N), sulfur (S), and variable elements. Chemoheterotrophy and aerobic chemoheterotrophy represented the most abundant inferred functional categories, with relative abundances ranging from 26.94% (SD) to 41.68% (BD) and 23.23% (SD) to 34.22% (B), respectively (Fig. 6a). Even after removing the *Synechococcus* sequences, several inferred light-associated categories, including phototrophy, photoautotrophy, photosynthetic cyanobacteria, and oxygenic photoautotrophy, were still detected. The combined relative abundance of these categories ranged from 6.93% (BD) to 38.69% (SD). Among the inferred functional categories, C-associated functions accounted for the largest proportion, with an average relative abundance of 88.48% (Fig. 6b). Following the 24-h incubation, the relative abundance of C-associated categories decreased by 3.22% and 3.30% in the Light and Dark group, respectively, whereas variable-associated categories increased by 35.27% and 31.64%, respectively. In contrast, S-associated categories showed relatively higher representation in the Light group (+ 29.25%), whereas N-associated categories were relatively more abundant in the Dark group (+ 53.23%). Direct comparison between the Light and Dark groups revealed only a marginal difference in C-associated categories (+ 0.08%), whereas N-associated categories were 31.49% lower and S-associated categories were 44.56% higher in the Light group than in the Dark group.

The gene sequences of *Synechococcus* and bacteria were annotated against the KEGG database. A heatmap based on the 50 enzymes with the highest average relative abundance illustrated differences in the relative representation of annotated enzyme-related genes among treatments under contrasting light conditions (Fig. 6c and 6d). In *Synechococcus*, the 3 most abundant annotated enzymes were EC 7.1.1.2 (NAD(P)H-quinone oxidoreductase), EC 2.7.7.7 (DNA polymerase), and EC 1.9.3.1 (cytochrome c oxidase), whereas in bacteria the most abundant annotations were EC 2.7.7.7, EC 7.1.1.2, and EC 1.17.4.1 (ribonucleoside-diphosphate reductase). Compared with the ISR samples, differences in the relative representation of annotated enzyme-related genes were observed in both the Light and Dark treatments for *Synechococcus* and bacterial communities. Many annotated enzymes showing relatively higher representation under light conditions also exhibited similar patterns under dark conditions. In *Synechococcus*, these annotations were primarily involved in nucleic acid metabolism (e.g., EC 6.3.5.3, phosphoribosylformylglycinamidine synthase), transmembrane transport and ATP hydrolysis (e.g., EC 3.6.3.-), signal transduction (e.g., EC 2.7.13.3, histidine kinase), nutrient synthesis (e.g., EC 6.1.1.14, glycyl-tRNA synthetase), vitamin B_{12} metabolism (e.g., EC 2.5.1.17, cob(I)alamin adenosyltransferase), and redox reactions (e.g., EC 1.1.1.22, UDPglucose 6-dehydrogenase). In bacteria, these corresponding annotations were mainly associated with lipid metabolism (e.g., EC 2.3.1.9, acetyl-CoA C-acetyltransferase), amino acid metabolism (e.g., EC 6.2.1.1, acetyl-CoA synthetase), and energy metabolism (e.g., EC 1.3.5.4, fumarate reductase flavoprotein subunit).

When comparing the Light and Dark incubation conditions (Light vs. Dark groups), *Synechococcus* and bacterial communities showed distinct patterns in the relative representation of annotated enzymes. In *Synechococcus*, enzymes with increases under Light were mainly associated with carbon and carbohydrate metabolism, nucleotide biosynthesis, amino acid metabolism, and aminoacyl-tRNA biosynthesis. Representative annotations included aldehyde dehydrogenase (EC 1.2.1.3), phosphoribosylformylglycinamidine synthase (EC 6.3.5.3), 3-isopropylmalate/(R)-2-methylmalate dehydratase (EC 4.2.1.33/4.2.1.35), and several aminoacyl-tRNA synthetases. Under Dark, increasing enzymes were mainly associated with respiratory electron transport, central carbon metabolism, and nucleotide metabolism, including NADH dehydrogenase (EC 1.6.99.3), orotidine-5'-phosphate decarboxylase (EC 4.1.1.23), and cytochrome c oxidase (EC 1.9.3.1). In bacterial communities, enzymes with increases under Light were mainly related to carbohydrate and central carbon metabolism, amino acid and nucleotide metabolism, aminoacyl-tRNA biosynthesis, and DNA methylation, with UDP-glucose 4-epimerase (EC 5.1.3.2), DNA (cytosine-5)-methyltransferase (EC 2.1.1.37), and glucose-1-phosphate thymidylyltransferase (2.7.7.24) among the more prominent annotations. Under Dark, increasing enzymes were mainly associated with central carbon metabolism, respiratory and redox processes, lipid metabolism, and nucleotide and amino acid metabolism, including acetyl-CoA C-acetyltransferase (EC 2.3.1.9), NADH-quinone oxidoreductase (EC 1.6.5.3), succinyl-CoA synthetase (EC 6.2.1.5), and 3-oxoacyl-[acyl-carrier protein] reductase (EC 1.1.1.100).

Discussion

Response of Synechococcus to light conditions

The results showed that, except for BD in the dark treatment, *Synechococcus* relative abundance increased under both light (SL, BL) and dark (SD) conditions compared to their respective ISRs (S, B), suggesting a potential release from eukaryotic inhibition [36]. Short-term culture experiments highlighted the significant impact of light shifts on *Synechococcus* abundance, with responses varying based on the specific light transition. Notably, shifts from light to dark (SD vs. S) and dark to light (BL vs. B) led to substantial increases in *Synechococcus* abundance. Interestingly, the most pronounced *Synechococcus* proliferation occurred under complete darkness (SD), possibly due to the alleviation of photoinhibition and efficient repair of PSII. This allowed cells to restore photosynthetic capacity and maintain metabolic homeostasis, thereby fostering population growth under low-light or darkness conditions [37]. Furthermore, short-term fluctuations in light can influence the abundance of *Synechococcus* by modulating its photosynthetic efficiency and metabolic homeostasis. This phenomenon is consistent with its capacity to sustain growth via mixotrophic or heterotrophic pathways, thereby augmenting its proliferative potential under dark conditions [38, 39].

Among the 90 *Synechococcus* OTUs, OTU61, OTU415, and OTU483 were dominant, representing different S5.1 clades. Their relative abundances increased during light-dark transitions, particularly OTU61 (clade IX), which increased by 221.97% and 202.25% in SD vs. S and BL vs. B, respectively. These clade-specific responses suggest substantial ecological heterogeneity within *Synchococcus* and rapid adjustment to

fluctuating light availability. Such flexibility may benefit *Synechococcus* in the YRE, where tidal dynamics and turbidity frequently alter the underwater light environmrnt [40]. Conversely, minimal changes under stable light conditions (SL vs. S or BD vs. B) suggests that populations were already acclimated [41].

In this study, KEGG annotation of the metagenomic data showed that the 3 enzymes with the highest annotated abundance in *Synechococcus* across all samples were NAD(P)H-quinone oxidoreductase (EC 7.1.1.2), DNA-directed DNA polymerase (EC 2.7.7.7), and an oxidoreductase (EC 1.9.3.1). The persistent annotation of 3 enzymes across all treatment conditions suggests that they represent a core component of the *Synchococcus* functional gene repertoire, indicating that the genetic potential for baseline metabolic functions was maintained even in the absence of light. Light was associated with higher annotated abundance of enzymes linked to energy acquisition, nucleic acid biosynthesis, transmembrane transport, and redox reactions. This pattern is broadly consistent with the known role of photosynthesis in supplying ATP and NADPH to support carbon and nitrogen metabolism, redox regulation, and membrane transport [42], though whether these annotated differences reflect genuine shifts in cellular activity cannot be determined from metagenomic data alone.

Restructuring of the co-occurring bacterial community

Marine bacterioplankton communities and their predicted functions exhibited vertical differentiation, consistent with previous observations across depth-defined layers [43]. Although 1,112 OTUs were shared between surface (S) and bottom (B) samples, 1,077 and 993 OTUs were unique to each layer, respectively. After 24 h of incubation, OTU loss rates were higher in surface than bottom samples (57.72% vs. 46.51%), potentially reflecting the bottle effect [44], cycloheximide treatment, and altered environmental conditions. Bottom communitied remained more similar to *in situ* samples, whereas surface communities showed greater compositional displacement. These patterns suggest different degrees of community restructuring between water layers. From a functional perspective, light-associated responses may involve phototrophic taxa and proteorhodopsin (PR)-mediated energy acquisition by heterotrophic bacteria, which can enhance bacterial survival under starvation conditions [45]. Previous studies have documented diel oscillations in microbial transcripts and particulate metabolites in the surface ocean [46], while the prevalence of diel-cycling transcripts has been shown to decrease with depth [47]. These findings suggest that surface bacterioplankton may be more responsive to short-term environmental changes, whereas bottom communities may exhibit greater compositional stability over the 24-h incubation.

Notably, community shifts under both light and dark treatments showed broad similarity when compared with the *in situ* samples, suggesting that a substantial portion of the observed change reflects cultivation artifacts (spatial confinement, reduced turbulence, and altered nutrient dynamics) rather than to light itself [44]. Direct comparison between the light and dark treatments therefore provides a more interpretable basis for assessing light-associated effects, as both treatments shared the same enclosure conditions and differed only in illumination. Within this framework, Actinobacteria and Planctomycetes showed higher relative abundance under light relative to dark, whereas *α*-Proteobacteria declined and *γ*-

Proteobacteria increased. Although Actinobacteria lack functional photosystems, they possess photosensory proteins such as CryB-type cryptochromes that may enhance their capacity to exploit DOM released by primary producers under illuminated conditions [48], potentially contributing to their higher representation under light. Certain Planctomycetes, including relatives of Rhodopirellula baltica, exhibit tolerance to UVC radiation through DNA repair mechanisms [49], which may partly explain their persistence and enrichment under light treatment. The contrasting trends between *α*- and *γ*-Proteobacteria are broadly consistent with their differing ecological characteristics: *α*-Proteobacteria are generally associated with stable, low-nutrient conditions, whereas *γ*-Proteobacteria tend to respond more rapidly to pulses of labile organic matter such as those potentially released by photosynthetically active cells [50]. These results suggest that light was associated with compositional shifts in the bacterial community beyond those attributable to incubation effects alone, though the underlying mechanisms warrant further investigation.

Light- and incubation-associated dynamics of DOC

DOC exhibited a clear vertical gradient in the *in situ* samples, with concentrations in bottom waters averaging approximately 1.8-fold those in surface waters. This vertical pattern may reflect differences in organic-matter accumulation and transformation between the 2 layers. Such processes may be particularly relevant in this highly turbid YRE, where strong and frequent sediment resuspension can enhance disturbance and decomposition of sedimentary organic matter [51]. Microbial remineralization of particulate organic matter (POM) may further contribute to DOC pool, particularly in marginal seas where bacterial carbon demand can exceed the supply of recently released phytoplankton-derived carbon [52]. In addition, sediment desorption and pore-water release during resuspension in the turbidity maximum zone represent significant DOC sources in the YRE [53], which may contribute to the elevated DOC concentrations observed in bottom waters.

Following the 24-h incubation, DOC showed the largest change among the measured parameters, with net increases of 32.02, 37.96, 23.86, and 30.73 $mg \cdot L^{-1}$ in SL, SD, BL, and BD, respectively. This accumulation likely reflects a shift in the balance between DOC release and removal following enclosure. Reduced physical exchange with the surrounding environment limits dilution and export, while DOC-releasing processes may continue within the bottles, including bacterial extracellular hydrolysis of POM, cell leakage and lysis, and direct release from growing autotrophic prokaryotes such as *Synechococcus* [44, 54, 55]. Viral lysis may provide an additional source of dissolved organic substrates [56]. The continued released and transformation of organic matter under reduced physical exchange can tip the balance toward net DOC accumulation. Accordingly, the elevated DOC concentrations reflect an incubation-associated physical-biogeochemical response rather than a simple continuation of *in situ* DOC dynamics.

Against this incubation-associated background, comparison between the natural light and dark treatments provides an opportunity to assess whether light availability further contributed to DOC dynamics during the 24-h incubation. DOC concentrations were numerically higher under dark conditions than under natural light in both surface and bottom waters, but these differences were not statistically

significant. One possible explanation is that sunlight promotes photochemical transformation of DOM into low-molecular-weight and more biologically labile compounds, which can subsequently enhance microbial utilization and contribute to DOC removal [57]. Light availability has also been reported to enhance community-level DOC uptake, the magnitude of uptake also depended on salinity [58]. In parallel, light-dark transitions can regulate intracellular carbon metabolism in cyanobacteria through CP12-mediated regulation of the Calvin and oxidative pentose phosphate pathways [59]. Nevertheless, the 24-h incubation showed a directional tendency toward higher DOC concentrations under dark conditions, but not a statistically detectable effect of light availability on the bulk DOC pool. Longer-term or time-resolved incubations would be needed to determine whether this directional pattern develops into measurable changes in DOC dynamics.

Potential roles of Synechococcus-bacteria interactions in elemental cycling

Synechococcus and heterotrophic bacteria play important roles in marine elemental cycling, particularly through the coupling of carbon and nutrient transformations [60, 61]. In this study, metabolomic profiles showed a clear separation between the *in situ* seawaters and 24-h incubation groups, whereas only 9 metabolites differed between the Light and Dark treatments, suggesting that incubation-associated changes were more extensive than those associated with light availability. Several metabolites differed between the Light and Dark treatments, while DOC concentrations were numerically higher under dark conditions but without a significant difference. This suggests that light availability may influence the composition of the DOM pool without substantially altering its bulk concentration. Such changes in individual DOM components may arise from differences in their production, transformation, or utilization, and the DOM pool represents a potential interface linking autotrophic carbon production by *Synechococcus* with heterotrophic bacterial utilization. Heterotrophic bacteria can selectively utilize different carbon substrates and rapidly adjust substrate uptake in response to changing substrate availability [9, 60]. Light-driven processes, including photoheterotrophic energy acquisiton and photochemical DOM transformation, may influence bacterial energy supply and organic substrate availability [22, 45, 57]. These processes provide a plausible framework in which light availability may modulate potential carbon coupling between *Synechococcus* and heterotrophic bacteria, although the specific direction and pathways of carbon transfer cannot be resolved from the pooled measurements.

Beyond the observed changes in DOM composition, KEGG enzyme annotations and FAPROTAX-based functional predictions provided complementary, exploratory insights into microbial functional potential associated with C-N-S elemental cycling under different light conditions. C-associated functions dominated the predicted profiles, a stronger influence of incubation on broad functional composition than of light availability. Nevertheless, Light and Dark treatments different in the representation of C-, N-, and S-associated functions, with lower N-associated but higher S-associated functions under Light conditions. The KEGG annotations provided finer-scale details of the light-associated functional shifts. In *Synechococcus*, enzymes annotations showing increases in Light were mainly related to carbohydrate metabolism, nucleotide biosynthesis, amino acid metabolism, and aminoacyl-tRNA biosynthesis, broadly consistent with light-dependent metabolic reorganization involving carbon and biosynthetic [62]. In

contrast, annotations showing increases under Dark included NADH dehydrogenase, cytochrome c oxidase, and other enzymes involved in central carbon metabolism, indicating enhancement of respiratory and redox-related functions under Dark. These contrasting patterns are consistent with previous evidence that cyanobacteria metabolic responses vary across light-dark cycles, including changes in respiratory gene expression in marine *Synechococcus* [63]. A similar functional differentiation was observed in bacterial communities. Under Light, increased enzyme annotations were mainly related to carbohydrate and central carbon metabolism, nucleotide and amino acid metabolism, aminoacyl-tRNA biosynthesis, and DNA methylation. Under Dark, increases mainly in annotations associated with central carbon metabolism, respiratory and redox processes, lipid metabolism, and nucleotide and amino acid metabolism. These contrasting profiles may reflect differences in the potential metabolic strategies of bacterial communities under light and dark conditions. Marine heterotrophic bacteria can use light-derived energy while utilizing substrates, and interactions between *Synechococcus* and heterotrophic bacteria may further influence these metabolic relationships [20, 64]. FAPROTAX and KEGG results indicate that light availability may selectively modify microbial functional potential involved in carbon processing, nitrogen-containing biosynthesis, and sulfur-related metabolism, potentially contributing to variation in C-N-S cycling. However, these annotations represent functional potential rather than direct measurements of elemental transformation.

The inorganic nutrient data provide an additional, but more indirect, perspective on these potential elemental linkages. Under in situ conditions, vertical differences in NO_3^-, NO_2^-, NH_4^+, PO_4^{3-}, and SiO_3^{2-} concentrations were observed among the 3 stations, indicating spatial heterogeneity in nutrient availability within the estuarine water column. Such vertical contrasts are consistent with evidence that nutrient availability and microbial community composition can vary substantially across environmental gradients, with different microbial groups exhibiting distinct nutrient-acquisition strategies [65]. In contrast, the 24-h incubation produced only relatively small differences in inorganic nutrient concentrations, with particularly limited variation in NO_2^-. The weak response contrasts with the clearer changes observed in microbial community composition, metabolite profiles, and functional potential. Such a pattern may indicate that microbial restricting and changes in metabolic potential occur more rapidly than detectable shifts in bulk nutrient concentrations during short-term incubations. This interpretation is consistent with evidence that nitrogen transformation can proceed through temporally separated stages, with organic matter consumption and ammonium accumulation preceding subsequent nitrite and nitrate production [66]. The observed nutrient patterns should not be interpreted as direct evidence of light-driven nutrient uptake or remineralization, but rather as evidence that short-term microbial responses may occur without measurable changes in surrounding inorganic nutrient pools. This caution is further supported by evidence that bacterial transporter gene expression responds to dissolved organic carbon availability, while such expression does not directly quantify realized substrate uptake fluxes [67]. The vertical nutrient and DOC gradients observed *in situ* further suggest that these potential microbial interactions occur within a spatially heterogeneous nutrient environment, where the availability of organic and inorganic substrates may vary substantially between surface and bottom waters.

Based on the observations from KEGG-based enzyme-level annotation, metabolomics, DOC, and inorganic nutrient measurements under Light and Dark incubation conditions, a conceptual model was developed to illustrate how changes in light availability may reshape the potential metabolic coupling between *Synechococcus* and heterotrophic bacteria and thereby influence pathways associated with elemental cycling (Fig. 7). Under Light, photosynthetic activity of *Synechococcus* may provide recently fixed organic carbon and associated dissolved metabolites that could support or modify bacterial heterotrophic metabolism. The representation of functions associated with carbohydrate, amino acid, nucleotide, and aminoacyl-tRNA metabolism in both *Synechococcus* and bacteria, together with light-dependent shifts in enzyme-level functional profiles, suggests potential processes of organic-substrate transfer and transformation within the microbial assemblage. Changes in predicted bacterial functional categories further suggest that this potential metabolic coupling may extend beyond carbon processing to functions associated with nitrogen and sulfur metabolism. Under Dark, the increased representation of NADH dehydrogenase, cytochrome c oxidase, and other respiratory or redox-related enzymes indicated a shift in the metabolic profile of *Synechococcus* toward respiratory energy metabolism, while bacterial functions associated with reparation, redox processes, lipid metabolism, and central carbon metabolism were also increased. This metabolic differentiation between Light and Dark suggests that changes in light availability may influence not only the amount of autotroph-derived organic carbon potentially available to the microbial assemblage, but also the pathways through which this carbon is metabolically processed. The relatively limited differences in inorganic nutrient concentrations after the 24-h Light and Dark incubations further suggest that metabolic responses may precede readily detectable changes in bulk nutrient pools.

Conclusion

The 24-h shipboard incubation provided an exploratory assessment of the responses of *Synechococcus* and co-occurring bacterial communities to light variation in the Yellow River Estuary (YRE). The relative abundance of *Synechococcus*, particularly OTU61 (S5.1 Clade IX), increased under both light and dark conditions, whereas OTU loss was greater in surface bacterial communities (57.72%) than in bottom communities (46.51%). Compared with *in situ* conditions, incubation-associated changes were greater in magnitude than light-associated changes, highlighting the importance of considering incubation effects and initial environmental conditions when interpreting short-term microbial responses. Metagenomic annotation revealed differences in the predicted functional profiles of *Synechococcus* and bacteria between Light and Dark treatments. Under light conditions, the relative representation of enzymes associated with carbohydrate, amino acid, nucleotide, and aminoacyl-tRNA metabolism increased, whereas dark conditions were associated with increased representation of respiratory and redox-related enzymes. 9 differential metabolites were identified between the Light and Dark treatments, although these metabolites could not be assigned to specific microbial groups. Changes in dissolved organic carbon (DOC) and inorganic nutrient concentrations provide additional information for interpreting microbial responses to light variation; however, the 24-h incubation period may have been insufficient to detect significant changes in some chemical parameters.

Declarations

Conflicts of Interest

The authors declare no conflicts of interest.

Funding

This study is financially funded by the National Natural Science Foundation of China (No. 42576259), the National Key Research and Development Program of China (No. 2024YFF0506902), the China Postdoctoral Science Foundation (No. 2024M763300), and the Shandong Provincial Natural Science Foundation (No. ZR2025QC1004).

Author Contribution

YZ contributed to the writing-original draft, visualization, methodology, investigation, data curation, conceptualization. TW contributed to the writing-review and editing, software, funding acquisition, methodology. JL contributed to the writing-review and editing, validation, supervision, project administration, investigation, funding acquisition, conceptualization. HG contributed to the writing-review and editing, methodology. SQ contributed to the writing-review and editing, supervision, resources, project administration, conceptualization.

Acknowledgement

This work has been supported by the Ocean Negative Carbon Emissions (ONCE) Program. Data and samples were collected onboard of R/V “Chuangxin Yi” implementing the open research cruise NORC 2022-304 supported by NSFC Shiptime Sharing Project (project number: 42149301). The data analysis is supported by High-Performance Computing Platform of Yantai Institute of Coastal Zone Research, Chinese Academy of Sciences.

Data Availability

The raw metagenomic sequences were deposited in the National Center for Biotechnology Information (NCBI, https://www.ncbi.nlm.nih.gov/) Sequence Read Archive (SRA) under accession number PRJNA1263415.

Open Access This article is licensed under a Creative Commons Attribution 4.0 International License, which permits use, sharing, adaptation, distribution and reproduction in any medium or format, as long as you give appropriate credit to the original author(s) and the source, provide a link to the Creative Commons License, and indicate if changes were made. The images or other third party material in this

article are included in the article's Creative Commons License, unless indicated otherwise in a credit line to the material. If material is not included in the article's Creative Commons License and your intended use is not permitted by statutory regulation or exceeds the permitted use, you will need to obtain permission directly from the copyright holder. To view a copy of this license, visit http://creativecommons.org/licenses/by/4.0/.

References

1. Kamykowski D (1974) Possible interactions between phytoplankton and semidiurnal inter. J Mar Res 32:65–87. https://doi.org/10.1357/002224074784513789
2. Tréguer P, Bowler C, Moriceau B, Dutkiewicz S, Gehlen M, Aumont O, Bittner L, Dugdale R, Finkel Z, Iudicone D, Jahn O, Guidi L, Lasbleiz M, Leblanc K, Levy M, Pondaven P (2018) Influence of diatom diversity on the ocean biological carbon pump. Nat Geosci 11:27–37. https://doi.org/10.1038/s41561-017-0028-x
3. Richter DH, Veron F (2016) Ocean spray: An outsized influence on weather and climate. Phys Today 69:34–39. https://doi.org/10.1063/pt.3.3363
4. Holtrop T, Huisman J, Stomp M, Biersteker L, Aerts J, Grébert T, Partensky F, Garczarek L, Woerd HJ (2021) Vibrational modes of water predict spectral niches for photosynthesis in lakes and oceans. Nat Ecol Evol 5:55–66. https://doi.org/10.1038/s41559-020-01330-x
5. Carvalho F, Fitzsimmons JN, Couto N, Waite N, Gorbunov M, Kohut J, Oliver MJ, Sherrell RM, Schofield O (2020) Testing the Canyon Hypothesis: Evaluating light and nutrient controls of phytoplankton growth in penguin foraging hotspots along the West Antarctic Peninsula. Limnol Oceanogr 65:455–470. https://doi.org/10.1002/lno.11313
6. Flombaum P, Gallegos JL, Gordillo RA, Rincón J, Zabala LL, Jiao N, Karl DM, Li WKW, Lomas MW, Veneziano D, Vera CS, Vrugt JA, Martiny AC (2013) Present and future global distributions of the marine Cyanobacteria *Prochlorococcus* and *Synechococcus*. PNAS 110:9824–9829. https://doi.org/10.1073/pnas.1307701110
7. Flombaum P, Wang W, Primeau FW, Martiny AC (2020) Global picophytoplankton niche partitioning predicts overall positive response to ocean warming. Nat Geosci 13:116–120. https://doi.org/10.1038/s41561-019-0524-2
8. Gonsior M, Powers L, Lahm M, McCallister SL (2022) New perspectives on the marine carbon cycle–the marine dissolved organic matter reactivity continuum. Environ Sci Technol 56:5371–5380. https://doi.org/10.1021/acs.est.1c08871
9. Ottesen EA, Young CR, Eppley JM, Ryan JP, Chavez FP, Scholin CA, DeLong EF (2013) Pattern and synchrony of gene expression among sympatric marine microbial populations. PNAS 110:E488–E497. https://doi.org/10.1073/pnas.1222099110
10. Cherrier J, Valentine S, Hamill B, Jeffrey WH, Marra JF (2015) Light-mediated release of dissolved organic carbon by phytoplankton. J Mar Syst 147:45–51. https://doi.org/10.1016/j.jmarsys.2014.02.008

11. Cory RM, Kling GW (2018) Interactions between sunlight and microorganisms influence dissolved organic matter degradation along the aquatic continuum. Limnol Oceanogr Lett 3:102–116. https://doi.org/10.1002/lol2.10060
12. Azam F, Fenchel T, Field JG, Gray JS, Meyer-Reil LA, Thingstad F (1983) The ecological role of water-column microbes in the sea. Mar Ecol Prog Ser 10:257–263. https://doi.org/10.3354/meps010257
13. Buchan A, LeCleir GR, Gulvik CA, González JM (2014) Master recyclers: features and functions of bacteria associated with phytoplankton blooms. Nat Rev Microbiol 12:686–698. https://doi.org/10.1038/nrmicro3326
14. Moore LR, Coe A, Zinser ER, Saito MA, Sullivan MB, Lindell D, Frois-Moniz K, Waterbury J, Chisholm SW (2007) Culturing the marine cyanobacterium *Prochlorococcus*. Limnol Oceanogr 5:353–362. https://doi.org/10.4319/lom.2007.5.353
15. Cole JK, Hutchison JR, Renslow RS, Kim YM, Chrisler WB, Engelmann HE, Dohnalkova AC, Hu D, Metz TO, Fredrickson JK, Lindemann SR (2014) Phototrophic biofilm assembly in microbial-mat-derived unicyanobacterial consortia: model systems for the study of autotroph-heterotroph interactions. Front Microbiol 5:109. https://doi.org/10.3389/fmicb.2014.00109
16. Malfatti F, Samo TJ, Azam F (2010) High-resolution imaging of pelagic bacteria by Atomic Force Microscopy and implications for carbon cycling. ISME J 4:427–439. https://doi.org/10.1038/ismej.2009.116
17. Ma X, Coleman ML, Waldbauer JR (2018) Distinct molecular signatures in dissolved organic matter produced by viral lysis of marine cyanobacteria. Environ Microbiol 20:3001–3011. https://doi.org/10.1111/1462-2920.14338
18. Beliaev AS, Romine MF, Serres M, Bernstein HC, Linggi BE, Markillie LM, Isern NG, Chrisler WB, Kucek LA, Hill EA, Pinchuk GE, Bryant DA, Wiley HS, Fredrickson JK, Konopka A (2014) Inference of interactions in cyanobacterial-heterotrophic co-cultures via transcriptome sequencing. ISME J 8:2243–2255. https://doi.org/10.1038/ismej.2014.69
19. Zheng Q, Suttle CA, Wang Y, Xie R, Lang AS, Liu Y, Lu J, Zhang X, Sun J, Jiao N (2018) Dynamics of heterotrophic bacterial assemblages within *Synechococcus* cultures. Appl Environ Microbiol 84:e01517–e01517. https://doi.org/10.1128/AEM.01517-17
20. Zheng Q, Wang Y, Lu J, Lin W, Chen F, Jiao N (2020) Metagenomic and metaproteomic insights into photoautotrophic and heterotrophic interactions in a *Synechococcus* culture. mBio 11:e03261–e03219. https://doi.org/10.1128/mBio.01511-19
21. Gomez-Consarnau L, Gonzalez JM, Coll-Llado M, Gourdon P, Pascher T, Neutze R, Pedros-Alio C, Pinhassi J (2007) Light stimulates growth of proteorhodopsin-containing marine *Flavobacteria*. Nature 445:210–213. https://doi.org/10.1038/nature05381
22. DeLong EF, Béjà O (2010) The light-driven proton pump proteorhodopsin enhances bacterial survival during tough times. PLoS Biol 8:e1000359. https://doi.org/10.1371/journal.pbio.1000359
23. Piwosz K, Villena-Alemany C, Mujakic I (2022) Photoheterotrophy by aerobic anoxygenic bacteria modulates carbon fluxes in a freshwater lake. ISME J 16:1046–1054.

https://doi.org/10.1038/s41396-021-01142-2

24. Liu S, Li L, Zhang G, Liu Z, Yu Z, Ren J (2012) Impacts of human activities on nutrient transports in the Huanghe (Yellow River) estuary. J Hydrol 430–431:103–110. https://doi.org/10.1016/j.jhydrol.2012.02.005
25. Bai J, Xiao R, Zhang K, Gao H (2012) Arsenic and heavy metal pollution in wetland soils from tidal freshwater and salt marshes before and after the flow-sediment regulation regime in the Yellow River Delta, China. J Hydrol 450–451:244–253. https://doi.org/10.1016/j.jhydrol.2012.05.006
26. Zhang J, Li F, Lv Q, Wang Y, Yu J, Gao Y, Ren Z, Zhang X, Lv Z (2021) Impact of the Water–Sediment Regulation Scheme on the phytoplankton community in the Yellow River estuary. J Clean Prod 294:126291. https://doi.org/10.1016/j.jclepro.2021.126291
27. Wang Y, Liu D, Lee K, Dong Z, Di B, Wang Y, Zhang J (2017) Impact of Water-Sediment Regulation Scheme on seasonal and spatial variations of biogeochemical factors in the Yellow River estuary. Estuar Coast Shelf Sci 198:92–105. https://doi.org/10.1016/j.ecss.2017.09.005
28. Glibert PM, Heil CA, Madden CJ, Kelly SP (2023) Dissolved organic nutrients at the interface of fresh and marine waters: flow regime changes, biogeochemical cascades and picocyanobacterial blooms —the example of Florida Bay. USA Biogeochemistry 164:229–255. https://doi.org/10.1007/s10533-021-00760-4
29. Paerl RW, Venezia RE, Sanchez JJ, Paerl HW (2020) Picophytoplankton dynamics in a large temperate estuary and impacts of extreme storm events. Sci Rep 10:22026. https://doi.org/10.1038/s41598-020-79157-6
30. Wang T, Chen X, Li JL, Qin S, Cui YL, Xu F (2021) The moderating role of population succession in the adaptive responses of *Synechococcus* assemblages: evidence from light intensity simulation experiment. Photosynthetica 59:587–599. https://doi.org/10.32615/ps.2021.050
31. Hood RD, Higgins SA, Flamholz A, Nichols RJ, Savage DF (2016) The stringent response regulates adaptation to darkness in the cyanobacterium *Synechococcus* elongatus. PNAS 113:E4867–4876. https://doi.org/10.1073/pnas.1524915113
32. Tremaine SC, Mills AL (1987) Inadequacy of the eucaryote inhibitor cycloheximide in studies of protozoan grazing on bacteria at the freshwater-sediment interface. Appl Environ Microbiol 53:1969–1972. https://doi.org/10.1128/aem.53.8.1969-1972.1987
33. Kanehisa M, Goto S, Sato Y, Kawashima M, Furumichi M, Tanabe M (2014) Data, information, knowledge and principle: back to metabolism in KEGG. Nucleic Acids Res 42:D199–205. https://doi.org/10.1093/nar/gkt1076
34. Bengtsson-Palme J, Hartmann M, Eriksson KM, Pal C, Thorell K, Larsson DG, Nilsson RH (2015) METAXA2: improved identification and taxonomic classification of small and large subunit rRNA in metagenomic data. Mol Ecol Resour 15:1403–1414. https://doi.org/10.1111/1755-0998.12399
35. Jing H, Wang R, Jiang Q, Zhang Y, Peng X (2020) Anaerobic methane oxidation coupled to denitrification is an important potential methane sink in deep-sea cold seeps. Sci Total Environ 748:142459. https://doi.org/10.1016/j.scitotenv.2020.142459

36. Callieri C, Amalfitano S, Corno G, Bertoni R (2016) Grazing-induced *Synechococcus* microcolony formation: experimental insights from two freshwater phylotypes. FEMS Microbiol Ecol 92:1–10. https://doi.org/10.1093/femsec/fiw154
37. Soitamo A, Havurinne V, Tyystjärv E (2017) Photoinhibition in marine picocyanobacteria. Physiol Plant 161:97–108. https://doi.org/10.1111/ppl.12571
38. Yan R, Zhu D, Zhang Z, Zeng Q, Chu J (2011) Carbon metabolism and energy conversion of *Synechococcus* sp. PCC 7942 under mixotrophic conditions: comparison with photoautotrophic condition. J Appl Phycol 24:657–668. https://doi.org/10.1007/s10811-011-9683-2
39. Ravindran S, Hajinajaf N, Kundu P, Comes J, Nielsen DR, Varman AM, Ghosh A (2024) Genome-scale metabolic model reconstruction and investigation into the fluxome of the fast-growing cyanobacterium *Synechococcus* sp. PCC 11901. ACS Synth Biol 13:3281–3294. https://doi.org/10.1021/acssynbio.4c00379
40. Dufour L, Garczarek L, Gouriou B, Clairet J, Ratin M, Partensky F (2024) Differential acclimation kinetics of the two forms of type IV chromatic acclimaters occurring in marine *Synechococcus* cyanobacteria. Front Microbiol 15:1349322. https://doi.org/10.3389/fmicb.2024.1349322
41. Mackey KR, Post AF, McIlvin MR, Saito MA (2017) Physiological and proteomic characterization of light adaptations in marine *Synechococcus*. Environ Microbiol 19:2348–2365. https://doi.org/10.1111/1462-2920.13744
42. Veaudor T, Blanc-Garin V, Chenebault C, Diaz-Santos E, Sassi JF, Cassier-Chauvat C, Chauvat F (2020) Recent advances in the photoautotrophic metabolism of cyanobacteria: biotechnological implications. Life 10:1–26. https://doi.org/10.3390/life10050071
43. Zhang Y, Li J, Cheng X, Luo Y, Mai Z, Zhang S (2018) Community differentiation of bacterioplankton in the epipelagic layer in the South China Sea. Ecol Evol 8:4932–4948. https://doi.org/10.1002/ece3.4064
44. Ionescu D, Bizic-Ionescu M, Khalili A, Malekmohammadi R, Morad MR, de Beer D, Grossart HP (2015) A new tool for long-term studies of POM-bacteria interactions: overcoming the century-old Bottle Effect. Sci Rep 5:14706. https://doi.org/10.1038/srep14706
45. Go´mez-Consarnau L, Akram N, Lindell K, Pedersen A, Neutze R, Milton DL, Gonzalez JM, Pinhassi J (2010) Proteorhodopsin phototrophy promotes survival of marine bacteria during starvation. PLoS Biol 8:e1000358. https://doi.org/10.1371/journal.pbio.1000358
46. Boysen AK, Carlson LT, Durham BP, Groussman RD, Aylward FO, Ribalet F, Heal KR, White AE, DeLong EF, Armbrust EV, Ingalls AE (2021) Particulate metabolites and transcripts reflect diel oscillations of microbial activity in the surface ocean. mSystems 6:e00896–e00820. https://doi.org/10.1128/mSystems.00896-20
47. Vislova A, Sosa OA, Eppley JM, Romano AE, DeLong EF (2019) Diel oscillation of microbial gene transcripts declines with depth in oligotrophic ocean waters. Front Microbiol 10:2191. https://doi.org/10.3389/fmicb.2019.02191

48. Maresca JA, Keffer JL, Hempel PP, Polson SW, Shevchenko O, Bhavsar J, Powell D, Miller KJ, Singh A, Hahn MW (2019) Light modulates the physiology of ponphototrophic actinobacteria. J Bacteriol 201:e00740–e00718. https://doi.org/10.1128/JB.00740-18
49. Viana F, Lage OM, Oliveira R (2013) High ultraviolet C resistance of marine Planctomycetes. Antonie Van Leeuwenhoek 104:585–595. https://doi.org/10.1007/s10482-013-0027-x
50. Pinhassi J, Berman T (2003) Differential growth response of colony-forming alpha- and gamma-proteobacteria in dilution culture and nutrient addition experiments from Lake Kinneret (Israel), the eastern Mediterranean Sea, and the Gulf of Eilat. Appl Environ Microbiol 69:199–211. https://doi.org/10.1128/AEM.69.1.199-211.2003
51. Yu Z, Wang X, Han G, Liu X, Zhang E (2018) Organic and inorganic carbon and their stable isotopes in surface sediments of the Yellow River Estuary. Sci Rep 8:10825. https://doi.org/10.1038/s41598-018-29200-4
52. Liu Y, Kang J, Huang Y, Xue C, Huang B (2026) Linking phytoplankton-derived dissolved and particulate carbon production to bacterial metabolism across physical dynamics in a subtropical marginal sea. J Geophys Research: Oceans 131. https://doi.org/10.1029/2026jc024071
53. Gu D, Zhang L, Jiang L (2009) The effects of estuarine processes on the fluxes of inorganic and organic carbon in the Yellow River Estuary. J Ocean Univ China 8:352–358. https://doi.org/10.1007/s11802-009-0352-x
54. Azam F, Malfatti F (2007) Microbial structuring of marine ecosystems. Nat Rev Microbiol 5:782–791. https://doi.org/10.1038/nrmicro1747
55. Zhang Z, Tang L, Liang Y, Li G, Li H, Rivkin RB, Jiao N, Zhang Y (2021) The relationship between two *Synechococcus* strains and heterotrophic bacterial communities and its associated carbon flow. J Appl Phycol 33:953–966. https://doi.org/10.1007/s10811-020-02343-6
56. Weinbauer MG, Griebler C, van Aken HM, Herndl GJ (2020) Viral infection of prokaryotic plankton during early formation of the North Atlantic Deep Water. Aquat Microb Ecol 84:175–189. https://doi.org/10.3354/ame01934
57. Moran MA, Zepp RG (1997) Role of photoreactions in the formation of biologically labile compounds from dissolved organic matter. Limnol Oceanogr 42:1307–1316. https://doi.org/10.4319/lo.1997.42.6.1307
58. Yannarell AC, Paerl HW (2007) Effects of salinity and light on organic carbon and nitrogen uptake in a hypersaline microbial mat. FEMS Microbiol Ecol 62:345–353. https://doi.org/10.1111/j.1574-6941.2007.00384.x
59. Tamoi M, Miyazaki T, Fukamizo T, Shigeoka S (2005) The Calvin cycle in cyanobacteria is regulated by CP12 via the NAD(H)/NADP(H) ratio under light/dark conditions. Plant J 42:504–513. https://doi.org/10.1111/j.1365-313X.2005.02391.x
60. Xia X, Zheng Q, Leung S, Wang Y, Lee P, Jing H, Jiao N, Liu H (2021) Distinct metabolic strategies of the dominant heterotrophic bacterial groups associated with marine *Synechococcus*. Sci Total Environ 798:149208. https://doi.org/10.1016/j.scitotenv.2021.149208

61. Zhao H, Zhang Z, Nair S, Li H, He C, Shi Q, Zheng Q, Cai R, Luo G, Xie S, Jiao N, Zhang Y (2024) Overlooked vital role of persistent algae-bacteria interaction in ocean recalcitrant carbon sequestration and its response to ocean warming. Global Change Biol 30:e17570. https://doi.org/10.1111/gcb.17570
62. Xiong Q, Feng J, Li ST, Zhang GY, Qiao ZX, Chen Z, Wu Y, Lin Y, Li T, Ge F, Zhao JD (2015) Integrated transcriptomic and proteomic analysis of the global response of *Synechococcus* to high light stress. Mol Cell Proteom 14:1038–1053. https://doi.org/10.1074/mcp.M114.046003
63. Zhang H, Tan Y, Zhou Y, Liu J, Xia X (2024) Light-dark fluctuated metabolic features of diazotrophic and non-diazotrophic cyanobacteria and their coexisting bacteria. Sci Total Environ 910:168702. https://doi.org/10.1016/j.scitotenv.2023.168702
64. Moran MA, Miller WL (2007) Resourceful heterotrophs make the most of light in the coastal ocean. Nat Rev Microbiol 5:792–800. https://doi.org/10.1038/nrmicro1746
65. Duhamel S, Björkman KM, Karl DM (2012) Light dependence of phosphorus uptake by microorganisms in the subtropical North and South Pacific Ocean. Aquat Microb Ecol 67:225–238. https://doi.org/10.3354/ame01593
66. Xie R, Wang Y, Chen Q, Guo W, Jiao N, Zheng Q (2020) Coupling between carbon and nitrogen metabolic processes mediated by coastal microbes in *Synechococcus*-derived organic matter addition incubations. Front Microbiol 11:1041. https://doi.org/10.3389/fmicb.2020.01041
67. Poretsky RS, Sun S, Mou X, Moran MA (2010) Transporter genes expressed by coastal bacterioplankton in response to dissolved organic carbon. Environ Microbiol 12:616–627. https://doi.org/10.1111/j.1462-2920.2009.02102.x

Figures

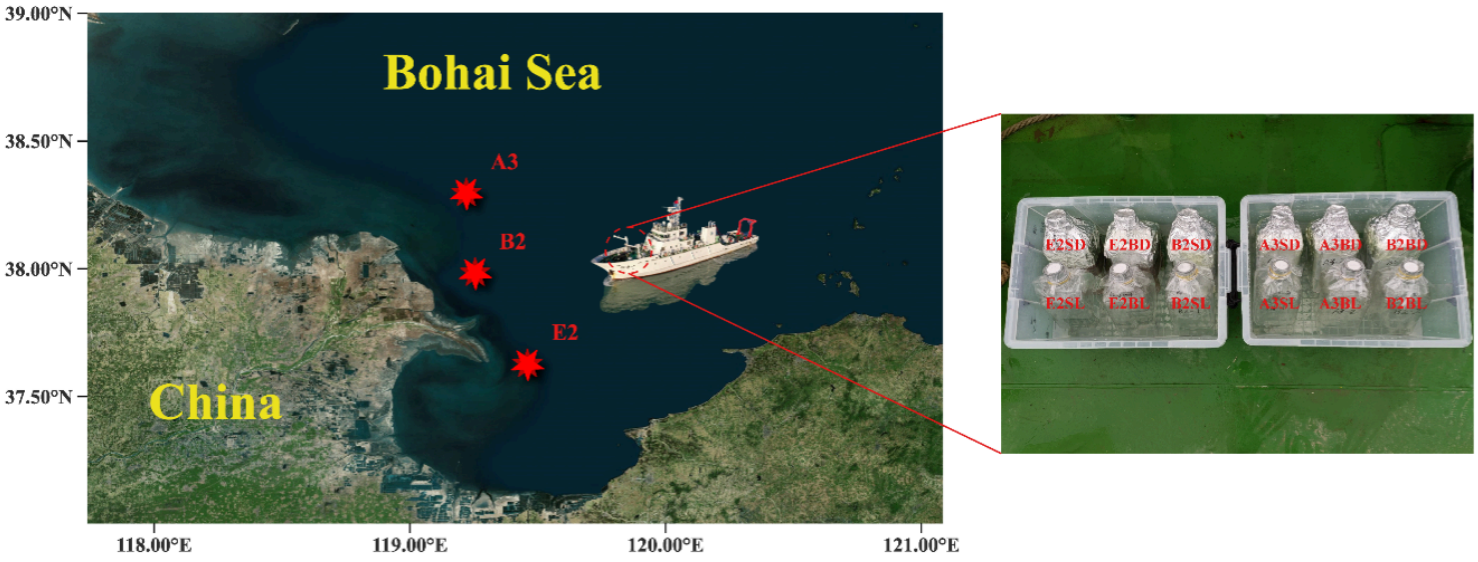

Figure 1

Map showing the locations of the studied sites and sampling stations. Left: Schematic map of the Yellow River Estuary, showing the locations of stations A3, B2, and E2. Right: Field photographs of the shipboard light-dark incubation experiments.

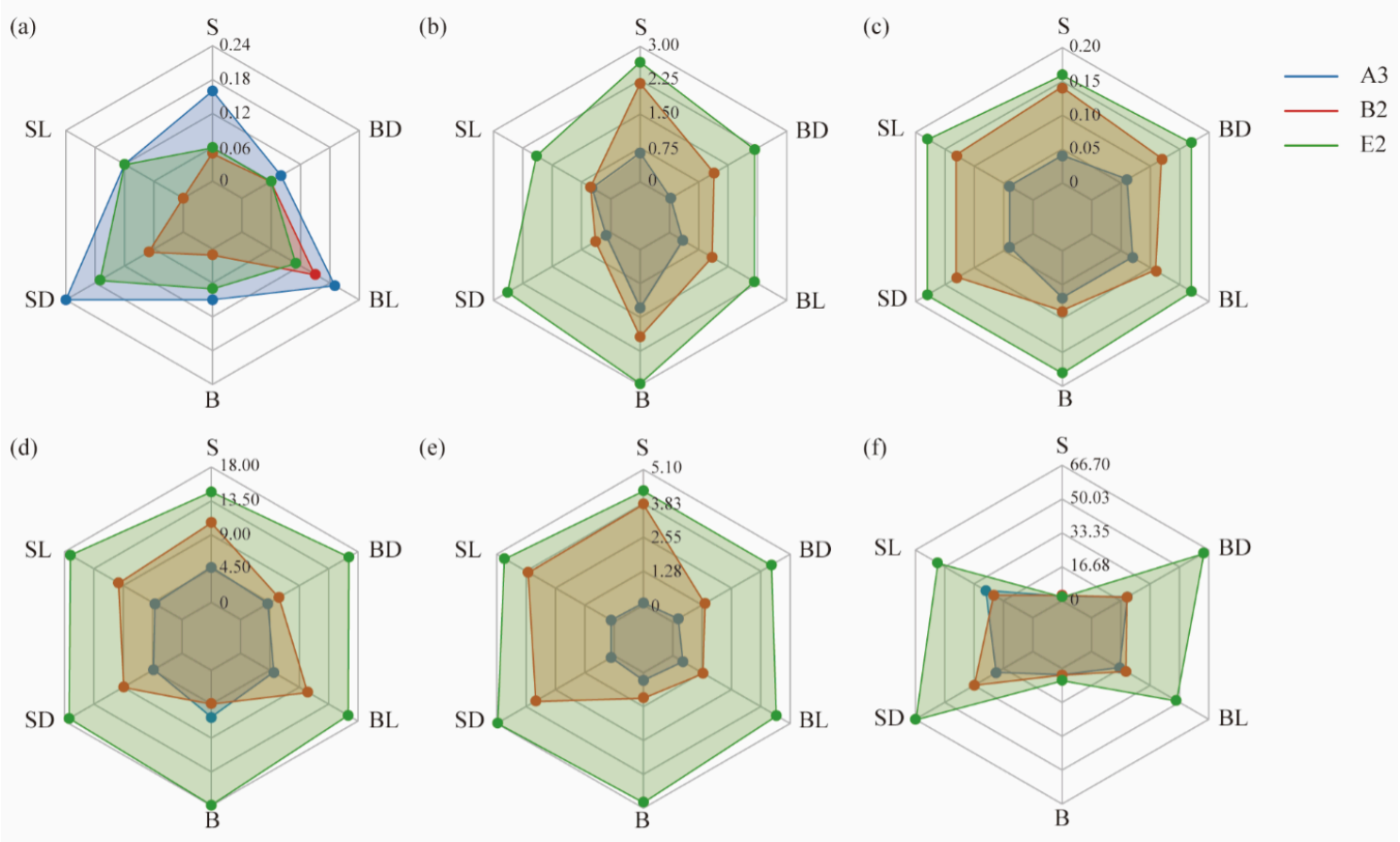

Figure 2

Nutrients and DOC concentration. Diagrams (a to f) represent the concentrations of phosphate (PO_4^{3-}; μmol•L⁻¹), ammonium (NH_4^+; μmol•L⁻¹), nitrite (NO_2^-; μmol•L⁻¹), silicate (SiO_3^{2-}; μmol•L⁻¹), nitrate (NO_3^-; μmol•L⁻¹), and dissolved organic carbon (DOC; mg•L⁻¹), respectively.

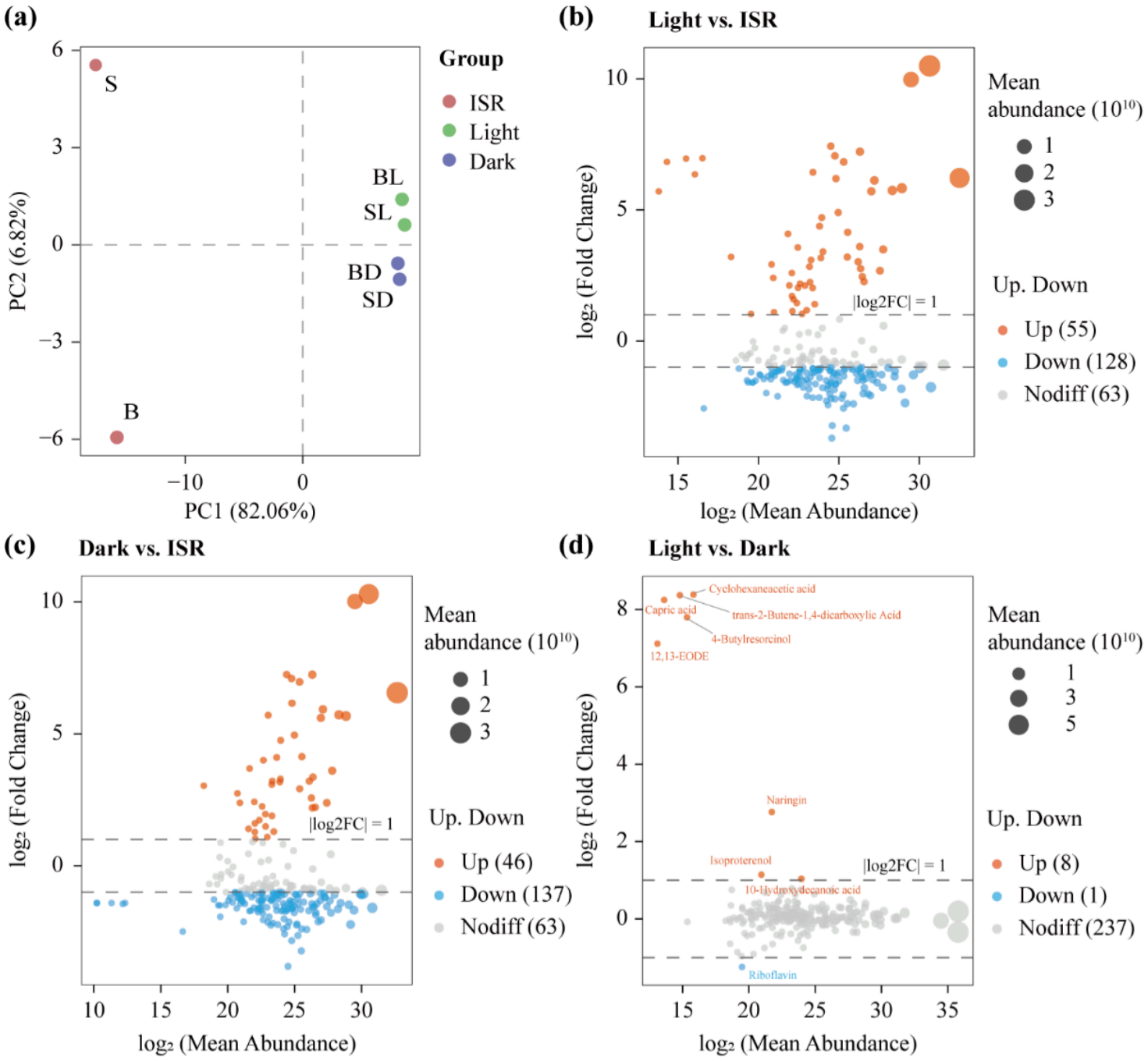

Figure 3

PCA score plots (a) of metabolomic profiles of 3 groups. MA plots (b) represents the comparisons between the Light group and the ISR group. Similarly, MA plots (c) and (d) illustrate the comparisons between the Dark and ISR groups, and the Light and Dark groups, respectively. Red dots represent the up-regulated metabolites. Green dots represent the down-regulated metabolites. Grey dots represent metabolites no difference.

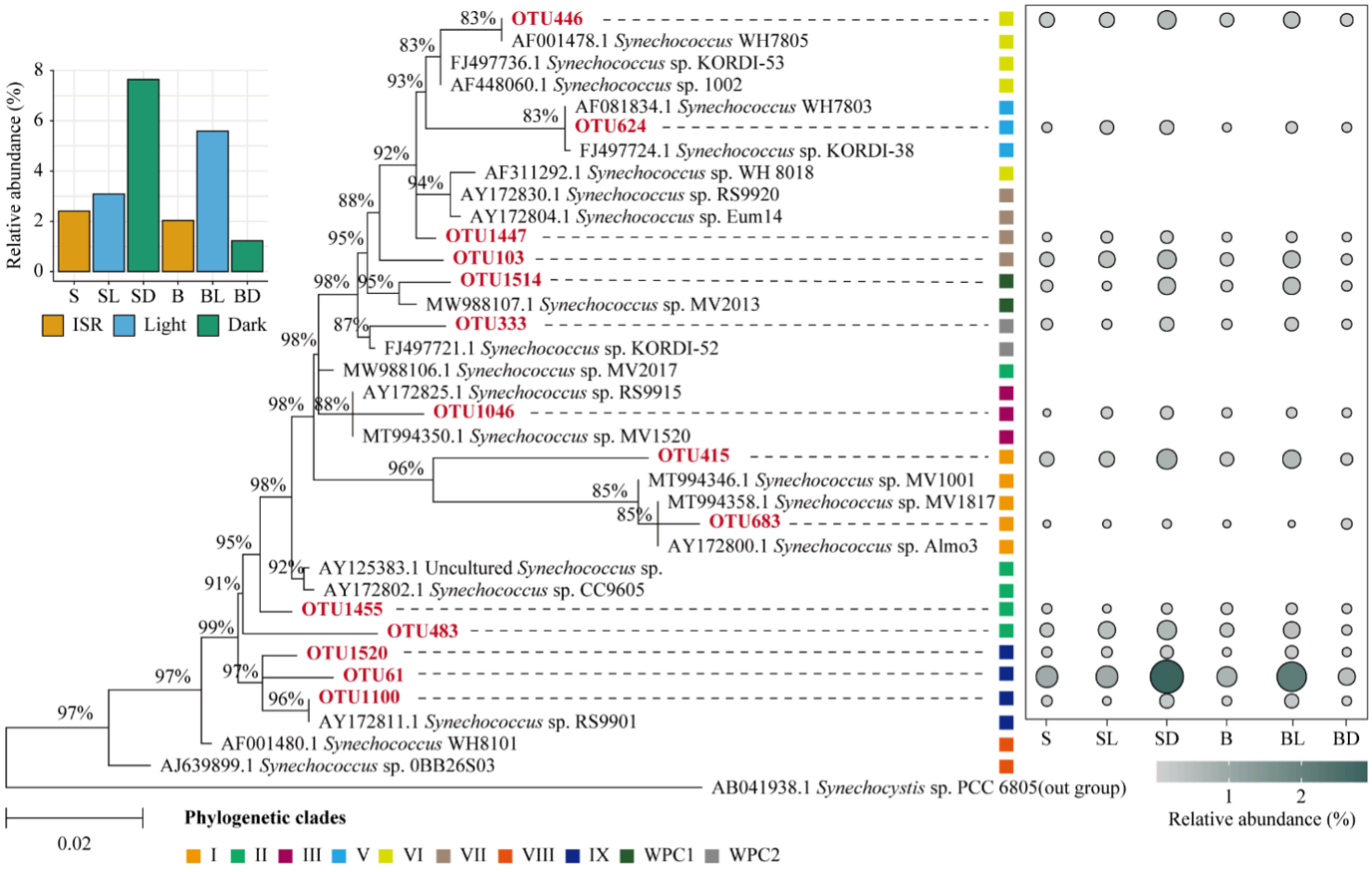

Figure 4

Phylogeny clades composition of *Synechococcus*. The bar plot represents the relative abundance (%) of *Synechococcus* in each sample. A maximum-likelihood phylogenetic tree of marine *Synechococcus* was constructed using 16S rRNA gene phylogenetically informative marker genes. *Synechocystis*sp. PCC7942 was employed as the outgroup. Distinctively colored nodes denote the clade assignment of each *Synechococcus* isolate.

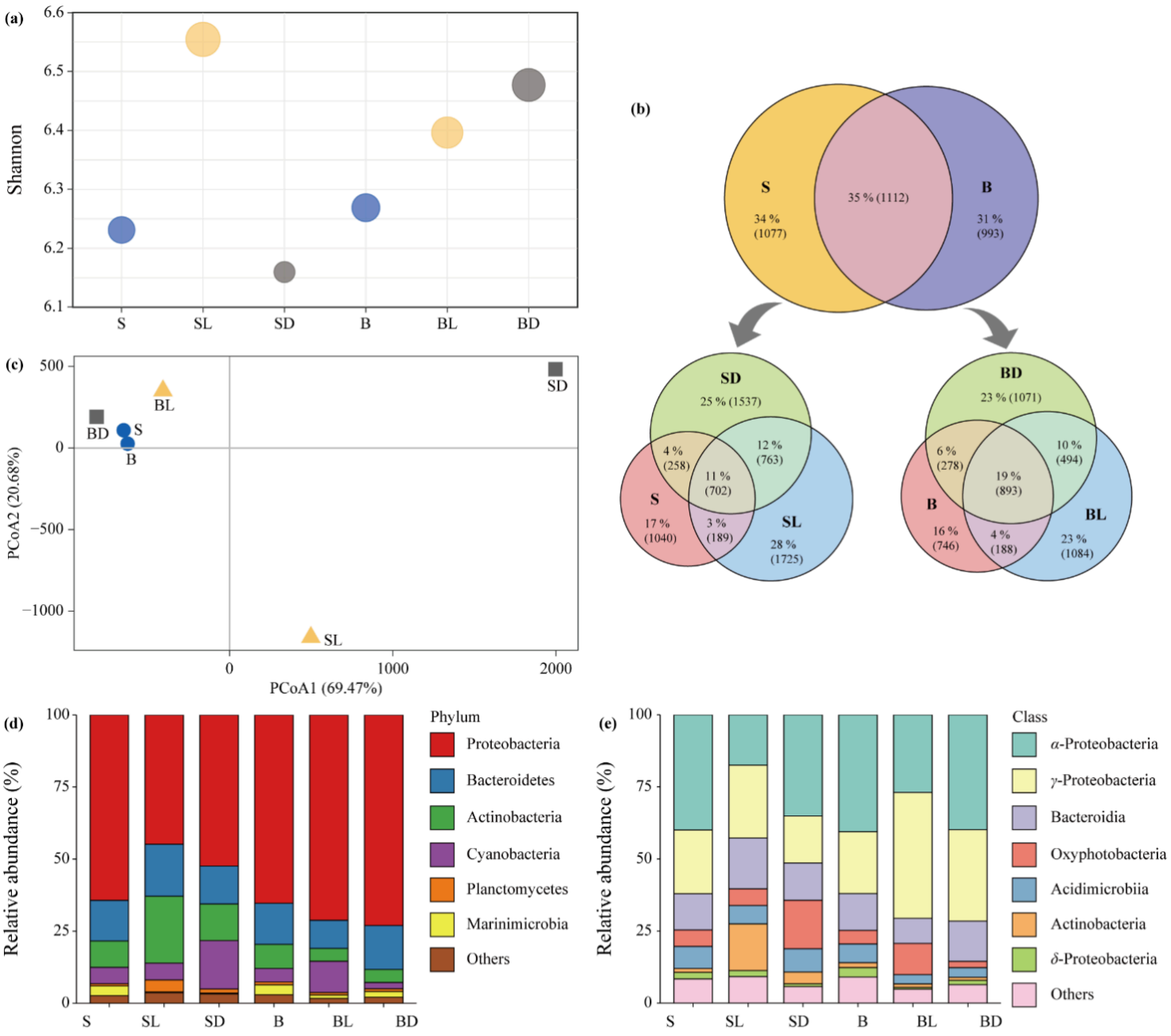

Figure 5

Diversity and community composition of bacteria based on 16S rRNA sequencing. Alpha diversity (a), Venn diagrams (b), and PCoA (c) about bacterial OTUs, and bacterial community at the Phylum (d) and Class (e) levels. Venn diagrams showing the shared and unique co-occurring bacterial OTU numbers after 24h incubation.

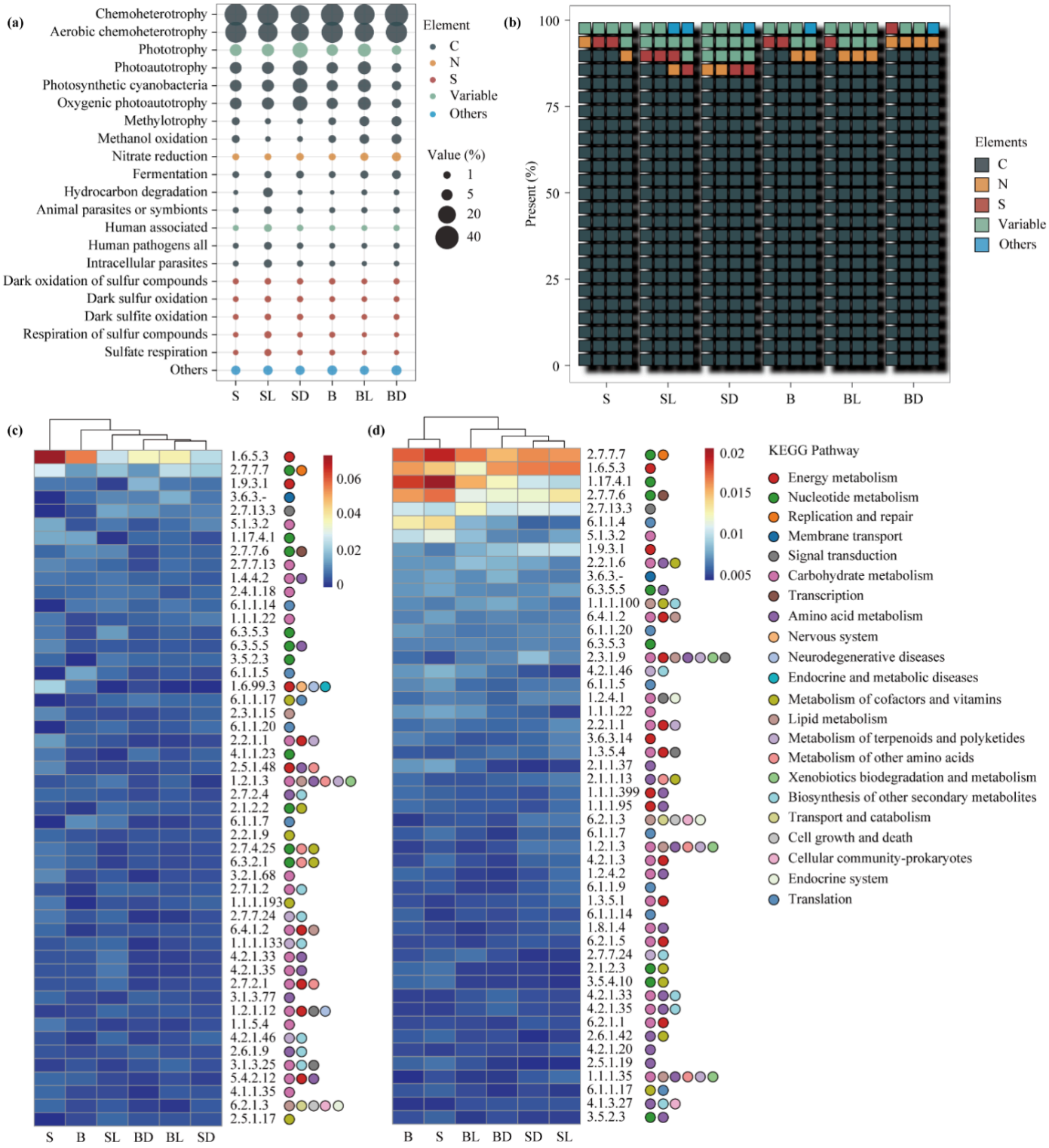

Figure 6

Functional annotations of *Synechococcus* and bacterial community. (a) FAPROTAX-predicted bacterial functional categories. (b) Relative proportions of element-associated functional categories. (c) Top 50 KEGG enzyme annotations in *Synechococcus*. (d) Top 50 KEGG enzyme annotations in bacteria. EC 1.6.5.3, now marked “obsolete” in KEGG and transferred to EC 7.1.1.2

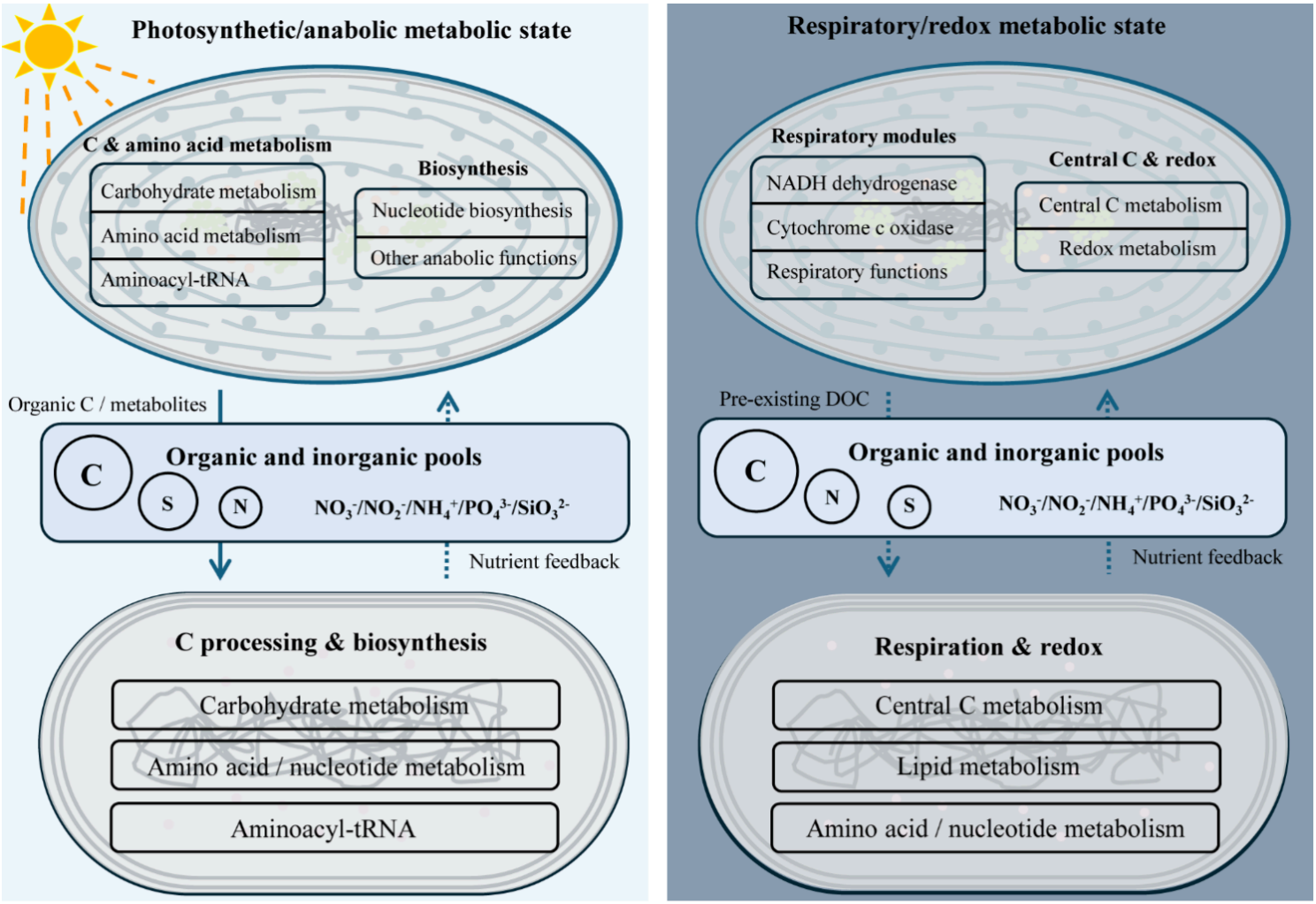

Figure 7

Conceptual model of potential *Synechococcus*-bacteria metabolic coupling under Light and Dark conditions

Supplementary Files

This is a list of supplementary files associated with this preprint. Click to download.

- TableS1.xlsx
- TableS2.xlsx
- TableS3.xlsx
- TableS4.xlsx
- TableS5.xlsx
- SupplementaryMaterial.docx